A problem to be solved for tungsten diagnostics through EUV spectroscopy in fusion devices

S.Morita[1,2], I.Murakami[1,2], H.A.Sakaue[1], C.F.Dong[1], M.Goto[1,2], D.Kato[1], T.Oishi[1,2], X.L.Huang[2] and E.H.Wang[2]

[1] National Institute for Fusion Science, Toki 509-5292, Gifu, Japan

[2] Department of Fusion Science, Graduate University for Advanced Studies, Toki 509-5292, Gifu, Japan

Abstract: Tungsten spectra have been observed from Large Helical Device (LHD) in extreme ultraviolet (EUV) wavelength ranges of 10-650Å. When the electron temperature is less than 2keV, the EUV spectra from plasma core are dominated by unresolved transition array (UTA) composing of a lot of spectral lines, e.g., 6g-4f, 5g-4f, 5f-4d and 5p-4d transitions for $W^{+24-+33}$ in 15-35Å. In order to understand the UTA spectrum, the EUV spectra measured from LHD plasmas are compared to those measured from Compact electron Beam Ion Trap (CoBIT), in which the electron beam is operated with monoenergetic energy of $E_e \leq 2$keV. The tungsten spectra from LHD are well analyzed based on the knowledge from CoBIT tungsten spectra. The collisional-radiative (C-R) model has been developed to explain the UTA spectra from LHD in details. Radial profiles of EUV spectra from highly ionized tungsten ions have been measured and analyzed by impurity transport simulation code with ADPAK atomic database to examine the ionization balance determined by ionization and recombination rate coefficients. If the electron temperature is higher than 2keV, Zn-like WXLV (W^{44+}) and Cu-like WXLVI (W^{45+}) spectra can be observed in LHD. Such ions of W^{44+} and W^{45+} can exhibit much simpler atomic configuration compared to other ionization stages of tungsten. Quantitative analysis of the tungsten density is attempted for the first time on the radial profile of Zn-like WXLV (W^{44+}) 4p-4s transition measured at 60.9Å, based on the emission rate coefficient calculated with HULLAC code. As a result, a total tungsten ion density of $3.5 \times 10^{10} cm^{-3}$ at the plasma center of LHD is reasonably obtained. Finally, the present problem for tungsten diagnostics in fusion plasmas is summarized.

1. Introduction

Recently, tungsten spectra have been widely studied in fusion research because the tungsten was adopted as divertor material of ITER instead of carbon which has been used for most of fusion devices [1-3]. At present, however, atomic data on the tungsten necessary for the impurity transport study are entirely insufficient [4-6]. The tungsten spectroscopy has been also started in Large Helical Device (LHD) by injecting carbon pellet included a small amount of tungsten [7].

Many tungsten line emissions have been measured so far from high-temperature tokamak plasmas in different wavelength ranges of EUV to visible light. At least, however, the spectral line which has been used for the plasma diagnostics is basically only one neutral tungsten line emitted at 4009Å [7]. Since the

tungsten line at 4009Å is well isolated from other lines and the line intensity is not so weak, it has been frequently used for studying the plasma wall interaction [8]. However, any quantitative analysis has not been done on the tungsten diagnostics in the plasma edge in addition to the plasma core. Then, a problem in studying the tungsten transport of fusion plasmas is summarized in the present paper.

2. Ionization energy of tungsten ions

Figure 1 shows the ionization energy of tungsten ions as a function of the charge state [9]. The electron temperature range in NBI discharges of LHD is indicated with gray hatched region. The highest charge state of tungsten ions which can be observed from LHD plasmas is probably Ni-like W^{46+}. Since the central temperature of ITER is very high as indicated with gray striped region, the atomic configuration of partially L-shell-ionized tungsten ions in the plasma core is simple and the impurity diagnostics using such ions is relatively easier. However, the partially N- and O-shell-ionized tungsten ions existing in the edge plasma of ITER still have many electrons in the bound orbit forming complicated atomic structure. The spectroscopic study of tungsten ions in LHD can give the information on such ions for the edge plasma diagnostics of ITER.

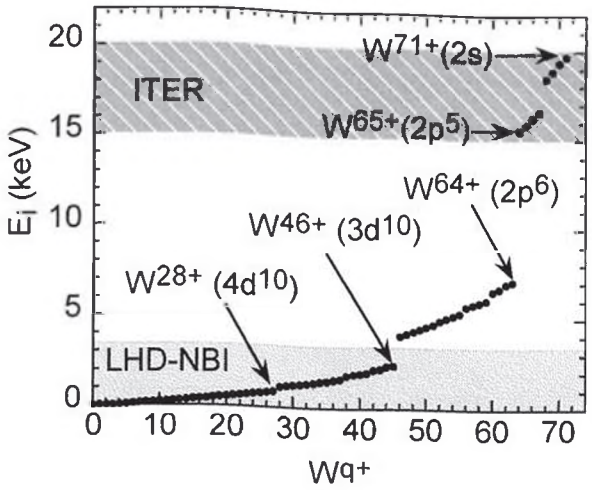

Fig.1 Ionization energy of W ions with charge state of q^+. Hatched and striped areas indicate electron temperature ranges at $T_e=E_i$ for NBI discharges in LHD and typical discharges in ITER, respectively.

The energy level among sublevels is illustrated in Fig.2 (a). In the impurity diagnostics the electric dipole transition as the resonance transition is usually measured for the impurity diagnostics of fusion plasmas due to the simple configuration. Then, the ionic sequence with one or two electrons in the outside bound orbit has been used for the diagnostics, i.e., H- or He-like, Li- or Be-like, Na- or Mg-like and so on. Looking at Fig. 2 (a) Pr- (W^{15+}) or Ce-like (W^{16+}) ions are also the good candidate for tungsten diagnostics. However, the ionization energies in such ions of W^{15+} and W^{16+} are entirely overlapped with those in partially 4f-subshell-ionized ions of W^{12+} and W^{27+}. The spectra from Pr- and Ce-like ions are not therefore simple due to the presence of several electrons in the outside bound orbit. The possible candidate for measuring the resonance transition in simpler ionic sequences is to use Zn- (W^{44+}) or Cu-like (W^{45+}) ions

for tungsten diagnostics. The 4p-4s resonance transition for such two ions illustrated in Fig.2 (b) becomes quite simpler compared to transitions for other ionization stages. Here, it should be noticed that the production of the W^{44+} and W^{45+} ions needs a relatively high electron temperature discharge as estimated from Fig.1.

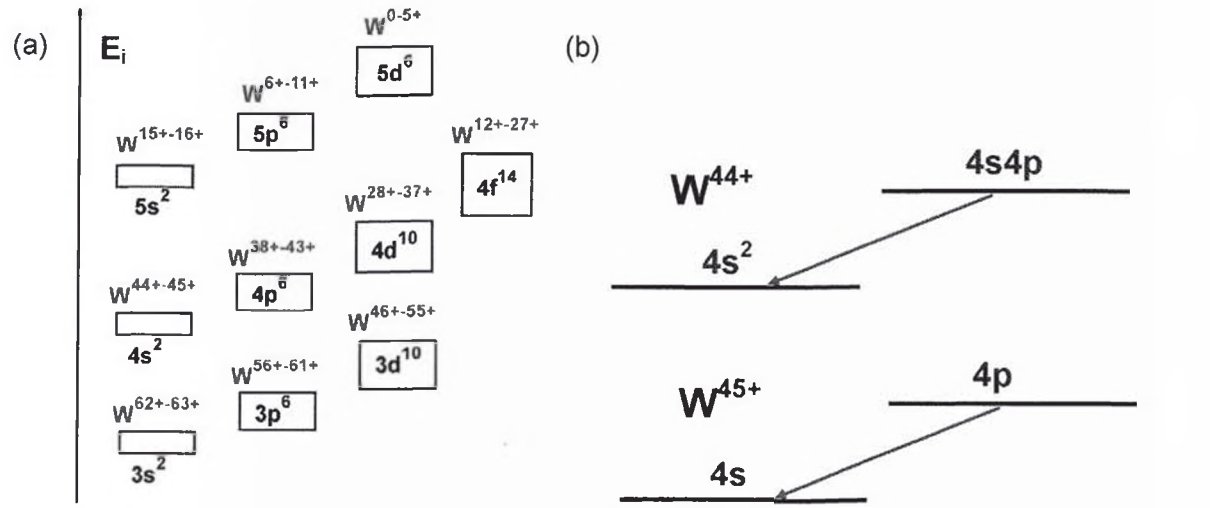

Fig.2 (a) Ionization levels of tungsten among sublevels and (b) 4p-4s resonance transitions for Zn-like W^{44+} and Cu-like W^{45+} ions. The ionization level of '4f' sublevel is overlapped with that of '5s' sublevel.

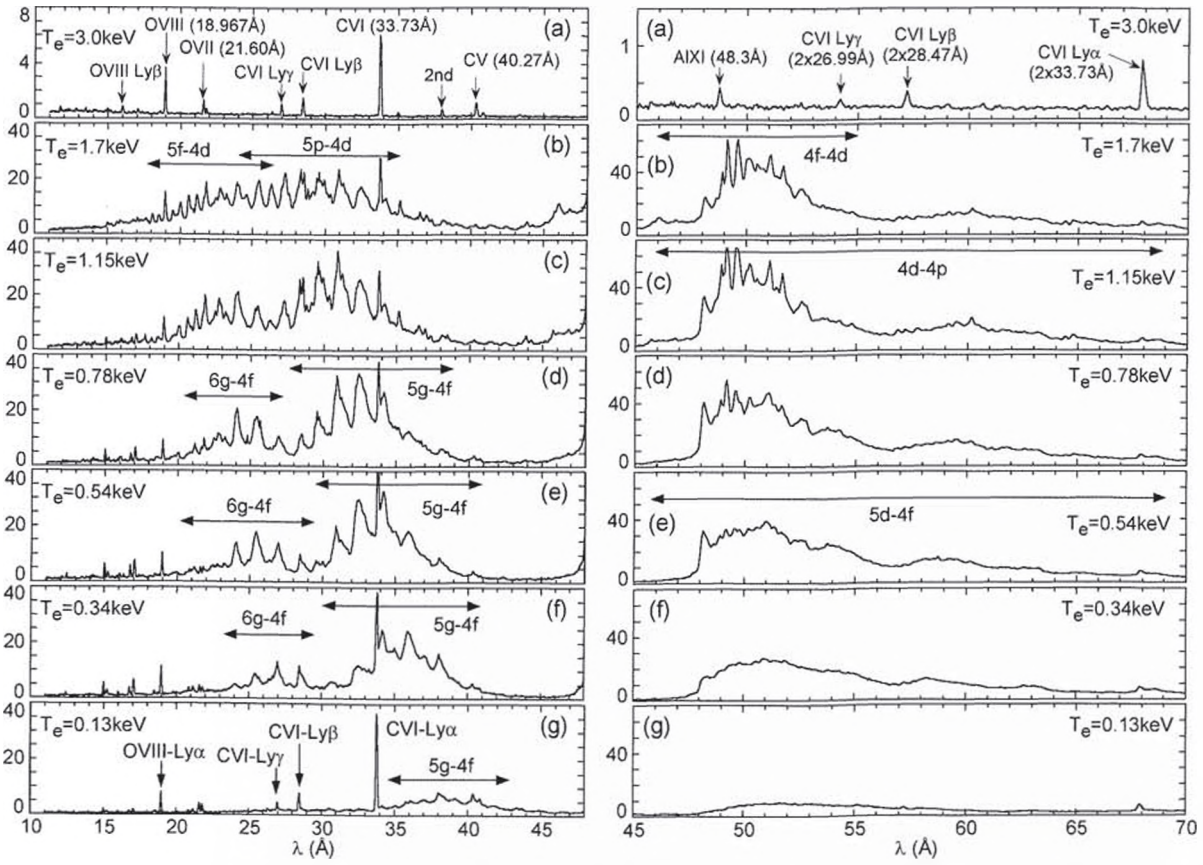

Fig.3 (a) LHD tungsten EUV spectra at 10-45Å (left) with 6g-4f, 5g-4f, 5f-4d and 5g-4f transitions in different electron temperatures of (b) 1.7keV, (c) 1.15keV, (d) 0.78keV, (e) 0.54keV, (f) 0.34keV and (g) 0.13keV and at 45-70Å (right) with 4f-4d, 4d-4p and 5d-4f transitions in different electron temperatures of (b)

1.7keV, (c) 1.15keV, (d) 0.78keV, (e) 0.54keV, (f) 0.34keV and (g) 0.13keV observed after carbon pellet injection with tungsten. Reference spectrum at T_e=3.0keV before pellet injection is plotted in (a). The 5d-4f transitions from W^{17+}-W^{27+} ions in 45-70Å interval are appeared at relatively low temperature range.

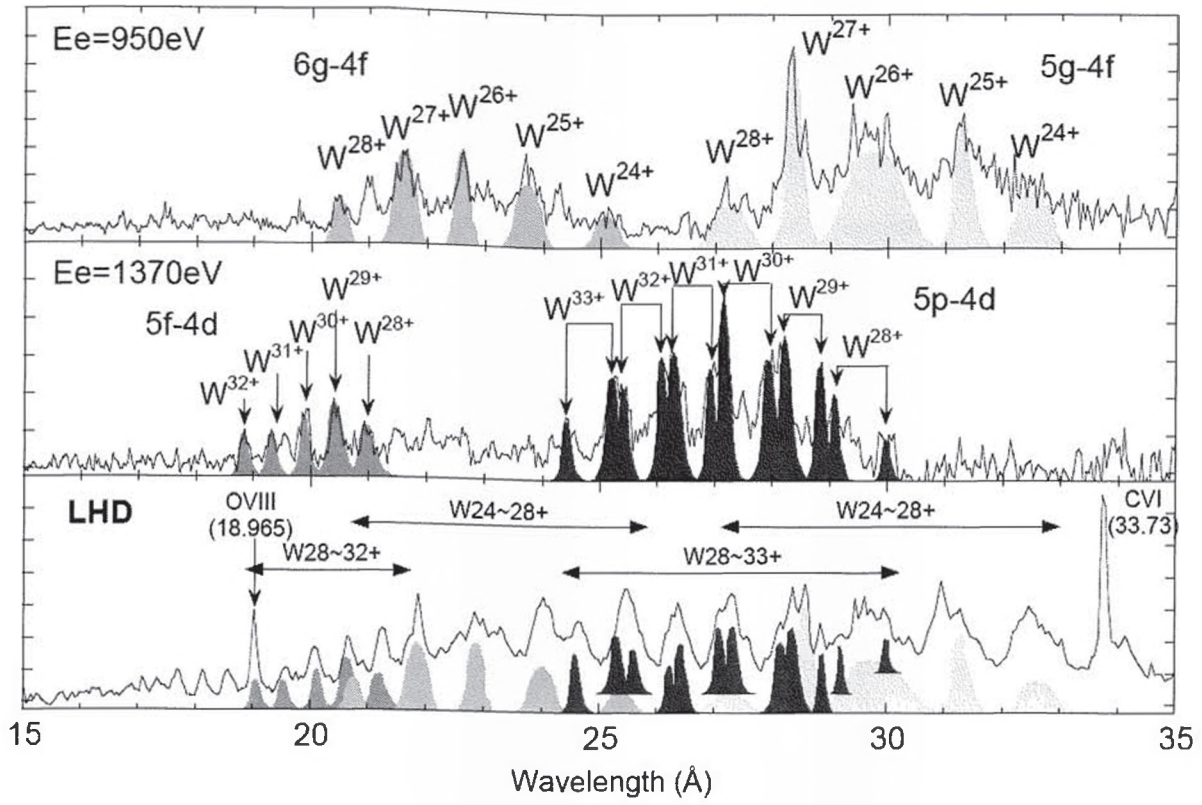

Fig.4 CoBIT tungsten EUV spectra with electron beam energies of (a) 950eV and (b) 1370eV, and (c) comparison between LHD EUV spectrum and composed spectrum of 6g-4f, 5g-4f, 5f-4d, 5p-4d transitions analyzed by HULLAC code against CoBIT spectra of (a) and (b).

3. EUV spectra from tungsten ions with lower ionization stages in LHD

A cylindrical carbon pellet ($1.2mm^{\phi}\times1.2mm^{L}$) with a small amount of tungsten enclosed in a narrow hole [10] is injected in NBI discharges to observe the tungsten spectra. The tungsten spectra measured from LHD using EUV spectrometers [11,12] are plotted in Fig.3 as a parameter of central electron temperature at two different wavelength ranges of 10-45Å (left) and 45-70Å (right). The EUV spectrum is recorded with sampling time of 5ms and a few frames are summed up for the plots. Several tungsten lines in such wavelength ranges have been already identified as earlier works [13]. The spectra observed before the pellet injection shown in Fig.3 (a) indicate He- and H-like emissions from intrinsic impurities of carbon and oxygen. The wavelength of tungsten emissions is determined using these lines. Since the Al pellet is injected in previous discharges, AlXI line is seen at 48.3Å.

The unresolved transition array (UTA) seen in Fig.3 (left) consists of the following transitions at various ionization stages of tungsten ions;

(1) 6g-4f (20-40Å) and 5g-4f (20-45Å)

transitions for $4s^24p^64d^{10}4f^q$ configurations

(2) 5f-4d (18-30Å) and 5p-4d (20-45Å) transitions for $4s^24p^64d^q$ configurations.

The shape of UTA changes with electron temperature because the radial location of tungsten ions also changes as a function of electron temperature. The transition array moves to longer wavelength side with decreasing electron temperature. It means that the tungsten emission from lower ionization stages exists in longer wavelength side, while the identification of each spectral line is entirely difficult due to the formation of UTA.

Similar UTA is also seen in Fig.3 (right), which consists of the following transitions;

(1) 4f-4d (45-55Å) and 4d-4p (45-70Å) transitions for $4s^24p^q4d^r4f^s$ configurations in W^{17+}-W^{43+} ions.

(2) 5d-4f (45-70Å) transitions for $4s^24p^64d^q4f^r$ configurations in W^{17+}-W^{27+} ions.

In order to analyze the UTA in 15-35Å the tungsten spectra are observed from CoBIT [14] working in NIFS. The EUV spectra from tungsten ions are shown in Figs.4 (a) and (b), which are observed at electron beam energies of 950 and 1370eV, respectively. The UTA are analyzed using HULLAC code with the presence of monoenergetic electrons. The results are also plotted in the same figures for the comparison. The EUV spectra observed from CoBIT are well explained by the present analysis with four transitions of 6g-4f, 5f-4d, 5f-4d and 5p-4d. The four transitions obtained from HULLAC code are compared with the LHD spectrum, as shown in Fig.4 (c). The contribution of each transition to the LHD spectrum is distinct, when the CoBIT spectra are used for the analysis on the LHD spectrum. We thus understand that the EBIT/CoBIT data are very useful for spectral analysis of high-Z elements in the fusion plasma.

The modeling of EUV spectra from highly ionized tungsten has been also developed in NIFS [15]. At present, the collisional-radiative (CR) model is constructed for tungsten ions (W^{q+}) with ionization stages of q=20 to 45, considering parameter range of LHD. Atomic data are calculated by HULLAC code under Maxwellian electron velocity distribution. In the present modeling the excited fine structure levels up to n=6 ($l \leq 5$) are considered, while the recombination process is not included. Therefore, the level population of 2,000-26,000 sublevels is examined for one ion.

4. Quantitative analysis of Zn-like (W^{44+}) tungsten

The Zn-like (W^{44+}) tungsten spectrum can be observed at 60.9Å if the electron temperature is higher than 2.3 keV, as shown in Figs.5 (a) - (e). The Zn-like tungsten is emitted with strong intensity in the range of $2.3 \leq T_e \leq 3.2$keV, but it begins to disappear when the electron temperature increases above 3.2keV, since the W^{44+} ion moves to outer side of the LHD plasma. The Zn-like tungsten at 60.9Å is a little blended with other lines at the shorter and longer wavelength sides. Ga-like tungsten (W^{43+}) exists at 60.5Å in shorter wavelength side of Zn-like tungsten. In the longer

wavelength side Ge-like (W^{42+}) and Ga-like (W^{43+}) tungsten also exist at 61.3Å. The detailed spectral structure near Zn-like tungsten [16] observed at T_e=2.90keV is shown in Fig.5 (f).

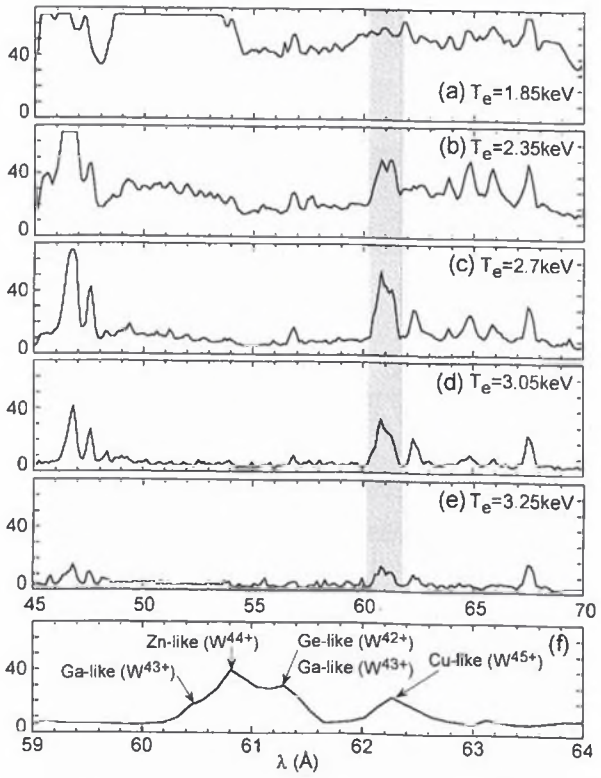

Fig.5 EUV spectra from Zn-like (W^{44+}: 60.9Å) tungsten ions at different electron temperatures of (a) 1.85keV, (b) 2.35keV, (c) 2.7keV, (d) 3.05keV and (e) 3.25keV. Hatched area indicates the vicinity of the Zn-like tungsten. Enlarged spectrum at T_e=2.90keV near Zn-like tungsten is plotted in (f).

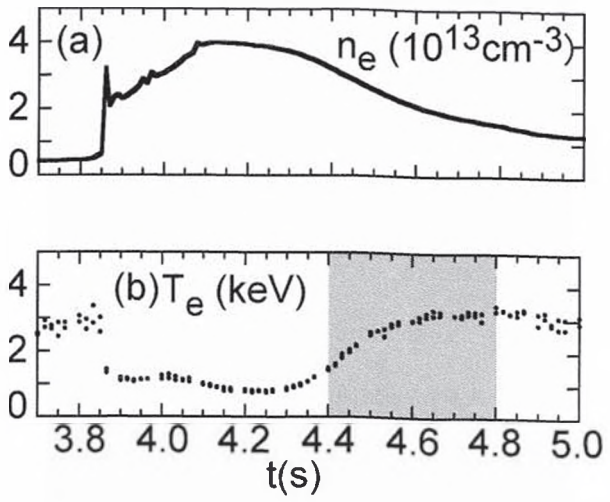

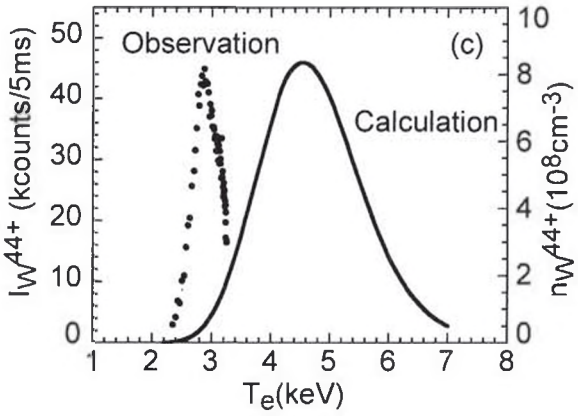

Fig.6 Waveforms of (a) electron density and (b) temperature after injection of cylindrical carbon pellet (1.2mm$^{\phi}$×1.2mm^{L}) with tungsten in LHD and (c) temperature dependence of Zn-like (W^{44+}) 4p-4s transition at 60.9Å (observation: solid circles and impurity transport calculation: solid line). The pellet is injected at 3.85s in NBI discharge and Zn-like tungsten is analyzed for 4.4-4.8s indicated with hatched area.

In order to examine the accuracy of the rate coefficients used in the impurity transport code the intensity of Zn-like tungsten is analyzed against the electron temperature using the temperature recovery phase after injection of the carbon pellet with tungsten. Electron density and temperature behavior after the impurity pellet injection is shown in Figs.6 (a) and (b), respectively. The density rise, Δn_e, after injection of tungsten-enclosed carbon pellet with size of 12.mm$^{\phi}$×1.2mm^{L} is Δn_e=2x10^{13}cm^{-3}, whereas the density rise is expected to be Δn_e=3x10^{13}cm^{-3} if all the particles of the pellet are fully confined in the plasma. The gradual increase in the density after the pellet injection from 3.87s to 4.07s is due to the change in the edge particle transport. When the edge temperature decreases in LHD, the edge particle confinement

increases because of the reduced particle screening in the edge stochastic magnetic field layer [17, 18]. After 0.45s from the pellet injection the electron temperature begins to recover since the electron density decreases. Although the density of tungsten ions after the pellet injection is not exactly known, at least, it gradually decreases as a function of time because the impurity confinement time roughly ranges in 0.2-1.0s at the plasma center.

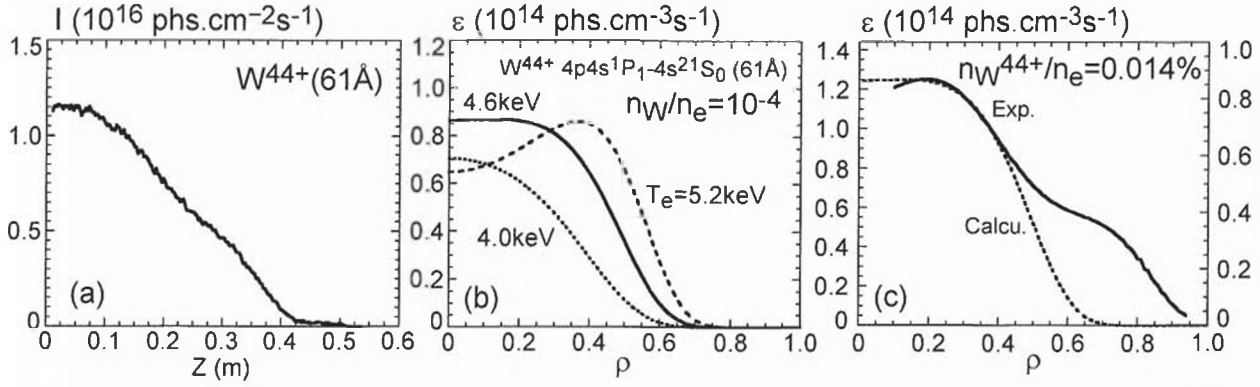

Fig.7 Observed vertical intensity profile and (b) calculated local emissivity profile of Zn-like (W^{44+}: 60.9Å) 4p-4s transition and (c) determination of W^{44+} ion density. The calculated local emissivity profile at T_e=4.6keV is used for the fitting to observed local emissivity profile.

The intensity of Zn-like tungsten is analyzed for the electron temperature recovery phase indicated with hatched area in Fig.6 (b). The result is plotted with solid circles in Fig.6 (c) as a function of central electron temperature. The Zn-like tungsten intensity evaluated from the present discharge takes the maximum value at T_e=2.8keV as a sharp function of electron temperature. The density of Zn-like tungsten calculated at the plasma center is also plotted in Fig.6 (c) with solid line. The electron temperature at which the n_W^{44+} takes the maximum is 4.5keV in the present impurity transport code. A large difference is clearly seen between the observation and the calculation. The reason definitely originates in a discrepancy in the ionization and recombination rate coefficients. The discrepancy of the rate coefficients from ADPAK code is studied for several ionization stages of tungsten [5]. The present result shows a similar tendency to the previous result, that is, the recombination rate of ADPAK is small compared to the experiment for Zn-like tungsten. However, several data from other ionization stages of tungsten are necessary to improve the impurity transport code by comparing the data between the present and previous results quantitatively. Radial intensity profile of Zn-like tungsten with 4p-4s transition at 60.9Å has been measured using a space-resolved EUV spectrometer in LHD [19]. The absolute sensitivity of the spectrometer is accurately determined using bremsstrahlung continuum from LHD [20]. A typical result is shown in Fig.7 (a). The centrally peaked profile indicates the Zn-like tungsten ion exists in the plasma center. In order to compare

with the impurity transport calculation, the chord-integrated vertical profile of Zn-like tungsten in Fig.7 (a) is reconstructed to the local emissivity profile using Abel inversion technique. The resultant profile plotted in Fig.7 (c) with solid line seems to have two components. It is probably an effect of the line blending with tungsten emission from ions in lower ionization stage. We need further examination on the Zn-like tungsten spectrum to conclude the true reason.

We calculate the emission coefficient of 4p-4s transition for the Zn-like tungsten based on HULLAC code. The radial emissivity profile of Zn-like tungsten is also calculated with different electron temperatures, as seen in Fig.7 (b). The emission location moves from the central region to the outside of plasma when the central electron temperature increases. In this calculation the tungsten ion density integrated along the whole plasma volume is assumed to be 10^{-4} to the electron density. In order to determine the tungsten density the measured local emissivity profile in Fig.7 (c) is compared with the transport calculation. The best fitting to the measured profile is obtained at T_e=4.6keV, as shown in Fig.7 (c) with dotted line. Of course, the temperature used in the present analysis is much different from the real temperature (T_e=2.8keV) because of the uncertainty of recombination rate. From this analysis the n_W^{44+} is estimated to be 1.4×10^{-4} to the electron density of $4\times10^{13}cm^{-3}$ at the plasma center. The total tungsten density in the plasma center can be then evaluated from n_W^{44+} to be $3.5\times10^{10}cm^{-3}$ ($n_W/n_e=8.8\times10^{-4}$). The total radiation loss, P_{rad}, is calculated with average ion model [21, 22] using the present tungsten density. We roughly estimate the value as P_{rad}=4MW. Since the measured P_{rad} in the present discharge ranges in 3-4MW after the tungsten pellet injection, the estimated P_{rad} from the present analysis seems to be reasonable.

5. Summary

Tungsten spectra in EUV wavelength range have been studied in LHD with radial distribution. Several problems are pointed out through the present study in addition to the previous works carried out in tokamaks if we study the impurity transport of tungsten ions. The subjects to be solved for the tungsten diagnostics are summarized in the following.

1. In relatively low-temperature range ($T_e \leq 2$keV) the EUV spectrum from tungsten is very complicated due to the appearance of UTA, which is not easy to analyze.
2. Collisional-radiative model has to be constructed to analyze the UTA structure.
3. A quantitative analysis of tungsten is possible in high-temperature range (T_e>2keV) when Zn-like (W^{44+}) or Cu-like (W^{45+}) ions are measured.
4. At present the tungsten transport study is entirely difficult due to a large uncertainty of the recombination rate.
5. Accuracy of the recombination rate has to be increased in addition to the wavelength.
6. The use of magnetic dipole transition (M1) is

alternative method to diagnose the tungsten ions by finding the good M1 line in visible or VUV range [23].

Acknowledgments

The authors wish to thank the LHD experiment team for their cooperation. This work was partially carried out under the LHD project financial support (NIFS12ULPP010). This work was partly supported by JSPS KAKENHI Grant Number 23340183 and the JSPS-NRF-NSFC A3 Foresight Program in the field of Plasma Physics (NSFC: No.11261140328).

References

[1] R.Stambaugh et al., Nucl. Fusion **39** (1999) 2391.

[2] R.Neu, R.Dux, A.Kallenbach, et al., Nucl. Fusion **45** (2005) 209.

[3] J.Roth, E.Tsitrone, T.Loarer et al., Plasma Phys. Control. Fusion **50** (2008) 103001.

[4] K.Asmussen, K.B.Fournier, J.M.Laming et al., Nucl. Fusion **38** (1998) 967.

[5] T.Putterich, R.Neu, R.Dux et al., Plasma Phys. Control. Fusion **50** (2008) 085016.

[6] J.Yanagibayashi, T.Nakano, A.Iwamae et al., J.Phys.B **43** (2010) 144013.

[7] S.Morita, C.F.Dong, M.Goto et al., to be published in AIP Conference Proceedings on 8th ICAMDATA, Gaithersburg (USA), 30 Sep. - 4 Oct. 2012.

[8] A.Thoma, K.Asmussen, R.Dux, et al., Phys. Control. Fusion **39** (1977) 1487.

[9] A.E.Kramida and T.Shirai Atomic Data Nucl. Data Tables **95** (2009) 305.

[10] R.Katai, S.Morita, M.Goto et al., Jpn. Soc. Appl. Phys. **46** (2007) 3667.

[11] M.B.Chowdhuri, S.Morita, M.Goto, et al., Rev.Sci.Instrum. **78** (2007) 023501.

[12] M.B.Chowdhuri, S.Morita and M.Goto Appl.Optics **47** (2008) 135.

[13] M.B.Chowdhuri, S.Morita and M.Goto Plasma Fusion Res. **2** (2007) S1060.

[14] H.A.Sakaue, N.Yamamoto, S.Morita, et al., J. Appl. Phys. **109** (2011) 073304.

[15] I.Murakami, N.Yamamoto, D.Kato, F.Koike, H.A.Sakaue and C.Suzuki, submitted to Plasma Fusion Res.

[16] T.Putterich, R.Neu, C.biedermann et al., J.Phys.B **38** (2005) 3071.

[17] M.B.Chowdhuri, S.Morita, M.Kobayashi et al., Phys.Plasmas **16** (2009) 062502.

[18] M.Kobayashi, S.Morita, C.F.Dong, et al., Nucl. Fusion **53** (2013) 033011

[19] C.F.Dong, S.Morita, M.Goto et al., Rev. Sci. Instrum. **81** (2010) 033107.

[20] C.F.Dong, S.Morita, M.Goto et al., Rev. Sci. Instrum. **82** (2011) 113102.

[21] D.E.Post and R.V.Jensen Atomic Data Nucl. Data Tables **20** (1977) 397.

[22] T.Putterich, R.Neu, R.Dux et al., Nucl. Fusion **50** (2010) 025012.

[23] D.Kato, M.Goto, S.Morita et al., to be published in Physica Scripta (2013).